J Mol Model (2010) 16:669–676
DOI 10.1007/s00894-009-0621-z

ORIGINAL PAPER

Ligand-based molecular design of 4-benzylpiperidinealkylureas and amides as CCR3 antagonists

Vaibhav Jain · Ashish Pandey · Shikhar Gupta · C. Gopi Mohan

Received: 9 September 2009 / Accepted: 26 October 2009 / Published online: 4 December 2009

Abstract Asthma is an inflammatory disease of the lungs. Clinical studies suggest that eotaxin and chemokine receptor-3 (CCR3) play a primary role in the recruitment of eosinophils in allergic asthma. Development of novel and potent CCR3 antagonists could provide a novel mechanism for inhibition of this recruitment process, thereby preventing asthma. With the intention of designing new ligands with enhanced inhibitor potencies against CCR3, a 3D-QSAR CoMFA study was carried out on 41 4-benzylpiperidinealkylureas and amide derivatives. The best statistics of the developed CoMFA model were r^2=0.960, r^2_{cv} = 0.589, n=32 for the training set and r^2_{pred} = 0.619, n= 9 for the test set. The generated 3D-QSAR contribution maps shed some light on the effects of the substitution pattern related to CCR3 antagonist activity.

Keywords 3D-QSAR · CoMFA · CCR3 antagonist · Asthma

Introduction

Eosinophils are granulocytes that reside predominantly within tissues. They possess several characteristic properties that promote inflammation, and their accumulation in the bronchial wall is a characteristic feature of asthma [1]. Once within the mucosa, degranulation of eosinophils releases granule constituents, such as major basic protein, eosinophil cationic protein, eosinophil derived neurotoxin, and eosinophil peroxidase along with several other cytokines that can cause tissue damage. These inflammatory mediators are thought to be one of the important aspects underlying bronchial hyper-reactivity leading to lung disease [2]. Eotaxin is the main chemokine produced in the lungs of asthmatic patients, and is a potent chemoattractant for eosinophils.

Chemokines are low molecular weight, structurally related, chemotactic cytokines that act on distinct subsets of leukocytes via specific G-protein-coupled receptors (GPCRs). Such chemokines are responsible for the activation, proliferation, and differentiation of leukocytes and hence play an important role in the control of basal leukocyte trafficking and recruitment of leukocytes during inflammation [3, 4].

Chemokines are classified mainly on the basis of the relative position of the conserved N-terminal cysteine residues found in their primary amino acid sequence. In CXC (α-chemokines), the pair of cysteines is kept apart by a single amino acid; CC (β- chemokines) feature adjacent cysteine residues; and in the CX3C (δ-chemokines) the first pair is separated by any three amino acids. In C (γ-chemokines) a single cysteine is usually present in the homologous position [5, 6]. Recent studies have suggested that chemokines are involved in a variety of pathophysiological processes, including acute and chronic inflammation like asthma, infectious diseases, and modulation of angiogenesis and fibrosis [7]. These chemokines bind to specific receptors, usually called chemokine receptors, which belong to class A GPCRs. Chemokine receptors are characterised by the presence of seven membrane-spanning helices and having high homology with rhodop-

Electronic supplementary material The online version of this article (doi:10.1007/s00894-009-0621-z) contains supplementary material, which is available to authorized users.

V. Jain · A. Pandey · S. Gupta · C. G. Mohan (✉)
Centre for Pharmacoinformatics,
National Institute of Pharmaceutical Education and Research,
Sector 67, S.A.S. Nagar,
160 062 Punjab, India
e-mail: cmohan@niper.ac.in
e-mail: cgopimohan@yahoo.com

sin, the prototypical family member. These receptors share common features with other members of the GPCR superfamily. All chemokine receptors have two conserved cysteine residues occupying the N-terminal domain and an extracellular loop 3, presumably forming a disulfide bridge, which is an integral part of the ligand-recognition site. In common with other superfamily members, there is a conserved DRY (Asp-Arg-Tyr) triad that resides at intracellular loop 2, indicative of a crucial function in G-protein binding [5]. The unique feature of the chemokine receptor subfamily is that all have an acidic N-terminus with gross negative charges ranging from −1 to −6, which may be involved in distinguishing the initial recognition event from other GPCRs. With the exception of the CXCR3 receptor, in all other chemokine receptors, two conserved acidic residues are also present within the helical bundle. The first of these residues, an Asp in helix 2, is closely associated with receptor activation as in all other GPCRs, and the second is a Glu residue in helix 7, which is involved in binding of monoamine ligands (unlike biogenic amine GPCRs, which have an Asp residue in helix 3). Alanine scanning mutagenesis of CCR3 revealed that two glutamate residues within the "EELFEET" motif of extracellular loop 2 of the receptor appear to be critical for trafficking of CCR3 to the cell membrane [8]. It was also shown that the conserved residues Y113 and E287 of CCR3 are important for the antagonist activity of compound UCB35625, and also for the agonist activity of eotaxin [9]. Moreover, four chemokine receptors—CXCR4, CCR5, CCR3, and CCR2b—have also been shown to have HIV-1 co-receptor activity [10, 11].

The dominant chemokine receptor found on eosinophils is CCR3, which, upon activation via eotaxin causes activation, proliferation, differentiation, and recruitment of eosinophils towards the site of inflammation. Stimulation of CCR3 by eotaxin has been shown to utilise the calcium-dependent tyrosine kinase pathway [phosphorylation of p38 mitogen-activated protein (MAP) kinases and extracellular signal-regulated kinase-2 (ERK2)], which appears to be an important upstream regulator for cell shape changes and cytoskeleton reorganisation [12, 13]. The amino-terminus of CCR3 appears to play a fundamental role in chemokine binding, whereas one or more of the extracellular loops are necessary for the effective relay of a signal to the cytoplasm [14]. Because of the prominent role of CCR3 in inflammation, agents that specifically block CCR3 function may be therapeutically useful, and information about the ligand binding site may help to develop novel efficacious blocking agents.

As no experimental structure is available for the CCR3 receptor, structure-based design is inapplicable, therefore ligand-based drug design approaches must be employed. *In silico* analysis of this receptor and its interaction with the ligand has been very limited to date. Using 141 CCR3 antagonists, Vedani et al. [15] developed a 5D-QSAR model based on a receptor-modeling concept. To the best of our knowledge, a survey of the literature has shown the latter study to be the only *in silico* study on CCR3 antagonists available to date.

Nowadays, 3D-QSAR techniques such as CoMFA and CoMSIA have been employed widely in computer-aided drug design. The contour maps generated from these models could not only help us to understand the mechanism of action of drug-receptor interaction, but could also served as a tool for designing potent inhibitors [16–20].

The structure-activity relationships of 4-benzylpiperidinealkylureas and amides with different C_4 substituents on the phenyl ring and urea N-H group revealed selective CCR3 antagonists. Addition of electronegative atoms such as chlorine or fluorine to the C_4 benzylpiperidine, and substitution of N–H group of urea with more lipophilic moieties increased CCR3 inhibition activity [21]. The present work deals with the CoMFA analysis of a series of 4-benzylpiperidinealkylureas and amides as CCR3 receptor antagonists, synthesised and tested at Bristol-Myers Squibb, Wilmington, DE [21].

Computational methods

Comparative molecular field analysis

3D-QSAR method comparative molecular field analysis (CoMFA) was introduced by Cramer et al. [22], and is based on the fact that the interaction between an inhibitor and its molecular target is primarily non-covalent in nature and shape dependent. Therefore, QSAR may be derived by sampling the steric and electrostatic fields surrounding a set of ligands and correlating the difference in these fields to biological activity. CoMFA calculates steric field using Leonard-Jones potential and electrostatic field using Coulomb potential.

Data set for CoMFA analysis

In vitro biological data of 4-benzylpiperidinealkylureas and amides as CCR3 antagonists reported by Wacker et al. [21] were used to construct a statistically significant CoMFA model and for the analysis of physico-chemical features. The structure and experimental values of activity (ranging from 0.005 μM to 1.6 μM) for the 41 molecules used in this study are shown in Table 1. The whole data set was divided into a training set of 32 molecules to generate the 3D-QSAR models, and a test set of 9 molecules (Table 1) to evaluate the predictive ability of the developed models. The structure and activity diversity in both the training and test set were considered for model development.

Table 1 Structures and activities of substituted 4-benzylpiperidinealkylureas and amides for comparative molecular field analysis (CoMFA) modeling

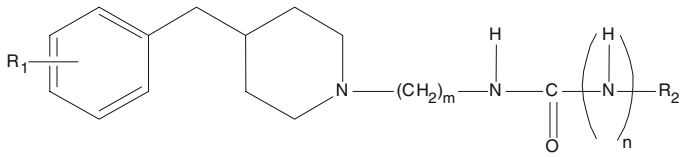

Molecule	R_1	m	n	R_2	[b]IC_{50} (μm)	pIC_{50}		Residual
						Actual	Predicted	
1	H	3	1	Ph	0.4	6.40	6.35	0.05
2	H	3	1	3-MeO-Ph	0.3	6.52	6.54	−0.02
3	H	2	1	3-CN-Ph	0.5	6.30	6.29	0.01
4	H	3	1	3-CN-Ph	0.2	6.70	6.81	−0.11
5[a]	H	4	1	3-CN-Ph	0.5	6.30	6.18	0.12
6	H	5	1	3-CN-Ph	1.2	5.92	6.01	−0.09
7	H	3	1	4-CF3-Ph	1.2	5.92	5.93	−0.01
8	H	3	1	4-Me_2N-Ph	1.6	5.80	5.76	0.04
9	4-F	3	1	Ph	0.03	7.52	7.43	0.09
10[a]	4-F	3	1	-CH_2Ph	0.4	6.40	7.41(5.84)	−1.01(0.56)
11	4-F	3	1	-CH_2CH_2Ph	0.3	6.52	6.57	−0.05
12	4-F	3	1	3-CN-Ph	0.02	7.70	7.91	−0.21
13	4-F	3	1	4-CN-Ph	0.02	7.70	7.76	−0.06
14	4-F	3	1	2-CF_3-Ph	0.2	6.70	6.63	0.07
15	4-F	3	1	3-CF_3-Ph	0.07	7.15	7.59	−0.44
16	4-F	3	1	4-CF_3-Ph	0.06	7.22	7.18	0.04
17	4-F	3	1	2-NO_2-Ph	0.089	7.05	7.14	−0.09
18[a]	4-F	3	1	3-NO_2-Ph	0.009	8.05	7.58	0.47
19	4-F	3	1	4-NO_2-Ph	0.007	8.15	7.56	0.59
20	4-F	3	1	3-Ac-Ph	0.01	8.00	7.71	0.29
21	4-F	3	1	4-Ac-Ph	0.2	6.70	6.91	−0.21
22	4-F	3	1	3-MeS-Ph	0.02	7.70	7.74	−0.04
23[a]	4-F	3	1	3-MeSO-Ph	0.05	7.30	7.71	−0.41
24	4-F	3	1	3-$MeSO_2$-Ph	0.02	7.70	7.67	0.03
25	4-F	3	1	4-MeS-Ph	0.04	7.40	7.40	0.00
26[a]	4-F	3	1	4-MeSO-Ph	0.2	6.70	7.29	−0.59
27[a]	4-F	3	1	4-$MeSO_2$-Ph	0.07	7.15	6.87	0.28
28	4-F	3	1	3-MeO-Ph	0.03	7.52	7.58	−0.06
29	4-F	3	1	3-(Furan-2-yl)-Ph	0.1	7.00	6.76	0.24
30	4-F	3	1	3-(Thiophen-2-yl)-Ph	0.2	6.70	6.89	−0.19
31	4-F	3	1	3-(Imidazol-2-yl)-Ph	0.1	7.00	6.80	0.20
32	4-F	3	1	3-(1-Me-tetrazol-5-yl)-Ph	0.005	8.30	8.32	−0.02
33	2-F	3	1	3-CN-Ph	0.2	6.70	6.67	0.03
34	4-Cl	3	1	3-CN-Ph	0.02	7.70	7.67	0.03
35[a]	4-Me	3	1	3-CN-Ph	0.5	6.30	7.20(5.85)	−0.90(0.45)
36	H	4	0	Ph	0.8	6.10	6.01	0.09
37[a]	H	4	0	3-MeO-Ph	1.2	5.92	5.73	0.19
38	H	4	0	4-CN-Ph	1.3	5.89	5.94	−0.05
39	H	4	0	4-F-Ph	1.0	6.00	6.04	−0.04
40	4-F	3	1	Adamant-1-yl	0.09	7.05	7.00	0.05
41[a]	4-F	3	1	Cyclohexyl	0.1	7.00	7.13	−0.13

[a] Molecules belonging to test set

[b] Experimental inhibitory activity of chemokine receptor-3 (CCR3) antagonist is taken from [21].

Molecular modeling

The molecules under study were built using the SYBYL7.1 molecular modeling package [23] installed on a Silicon Graphics Fuel Work station running IRIX 6.5. Since the crystal structure of the transmembrane domain of CCR3 is not available, and docking methodology could not be applied in order to obtain accurate bioactive conformation of the various ligands under study. Gasteiger-Hückel charges were applied to the atoms in the molecule for geometry optimisation. "Systematic search conformation" methodology was carried out to obtain a low energy conformer of the most potent molecule, **32** (IC_{50} value 0.005 μM), in gaseous phase. This minimum energy conformation of molecule **32** was then used as a template for building other molecules of the data set. The rest of the molecules were built by changing required substitution on the template molecule **32**, and energy minimizing only the modified part by the Powell method using Tripos force field, with 0.05 kcal mol^{-1} energy gradient convergence criterion, while keeping the atoms of the common scaffold frozen. These molecules were then used to construct a 3D-QSAR model. The IC_{50} value in the micro molar (μM) range was converted into the molar (M) range, and its logarithmic scale (pIC_{50}, M) was then used for subsequent QSAR analysis as the response variable.

Molecular alignment

Molecular alignment is the most sensitive parameter in 3D-QSAR analysis. CoMFA samples the steric and electrostatic fields surrounding a set of ligands and constructs a 3D-QSAR model by correlating the 3D fields with the corresponding biological/ experimental activities. One of the basic assumptions on which 3D-QSAR methodologies are based is that a geometric parallelism persists between the modelled structures and that of the bioactive conformation. This renders the spatial alignment of molecules under study as one of the most sensitive and determining factors in obtaining robust and meaningful QSAR models. The common substructure used for alignment, and the superimposed structure after alignment is presented in Fig. 1. In the present study geometry optimised molecules were aligned on the template molecule **32** (see Fig. 2) by common substructure alignment using the ALIGN DATABSE command in SYBYL. The lowest energy conformation of molecule **32** after systematic search has been taken as a template for alignment of the rest of the molecules in the data set.

CoMFA interaction energies

CoMFA electrostatic potential fields and steric fields were calculated at each lattice intersection on a regularly spaced grid of 2.0 Å units in the *x*, *y*, and *z* directions on the aligned data set. The pattern of the 3D cubic lattice generated automatically by the SYBYL/CoMFA routine extended at least 4.0 Å beyond the volumes of all investigated molecules along these axes. The van der Waals potential and Coulombic terms, representing steric and electrostatic fields, respectively, were calculated using the standard Tripos force field method. A distance-dependent dielectric constant of 1.0 was used and a sp^3 hybridized carbon atom with a +1 charge served as a probe atom to calculate steric and electrostatic fields. These field contributions were truncated to +30.0 kcal mol^{-1} and the latter were ignored at lattice intersections with maximal steric interactions [24].

Partial least squares analysis

The relationship between structural parameters (CoMFA interaction energies) and biological activities was quantified using the partial least squares (PLS) algorithm [25]. The cross-validation analysis was performed using the leave-one-out (LOO) method, where one molecule is removed from the data set and its activity is predicted using the model derived from the rest of the data set. The cross-validated r^2_{cv} that resulted in optimum number of components (NOC) and lowest standard error of prediction was selected. To speed up the analysis with reduced noise, a minimum column filtering value (σ) of 2.0 kcal mol^{-1} was used for cross-validation. Final analysis (non-cross-validation) was performed to calculate conventional r^2 using the

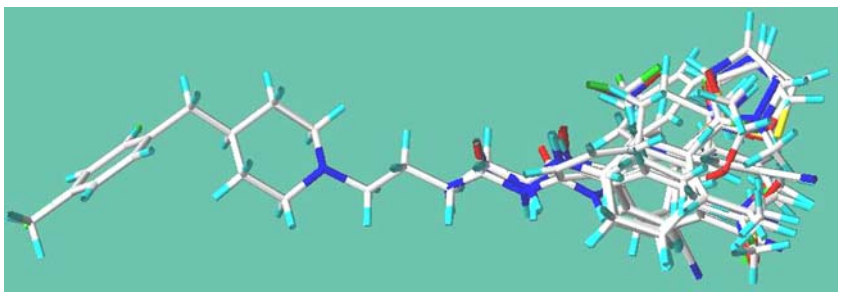

Fig. 1 Molecular alignment of 41 molecules

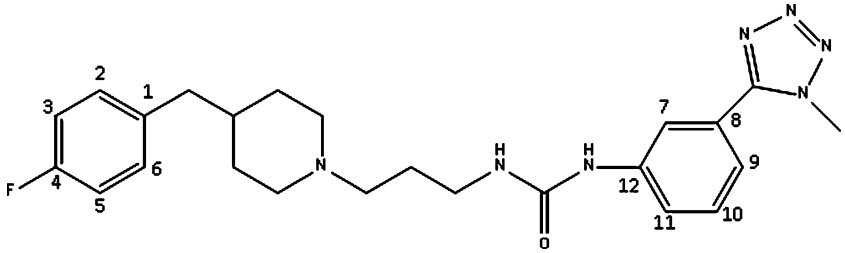

Fig. 2 Template molecule **32** with atom numbering

optimum NOC obtained from the LOO cross-validation analysis. To further assess the statistical confidence and robustness of derived 3D-QSAR model, boot strapping analysis [25] for 100 runs was performed.

Predictive correlation coefficient (r^2_{pred})

The predictive power of the 3D-QSAR models were determined from a set of nine molecules (test set) that were excluded during model development. The optimisation, alignment and all other steps for molecules of test set were the same as those adopted for training set molecules. The predicted activity of test set molecules was then computed with the CoMFA model developed from the training set molecules. The predictive correlation (r^2_{pred}) based on the test set molecules, is computed using Eq. 1.

$$r^2_{pred} = (SD - PRESS)/SD \quad (1)$$

Where SD is defined as the sum of the squared deviations between the biological activities of the test set, and the mean activity of training set molecules. PRESS is the sum of the squared deviation between the predicted and actual activity values for all molecules in the test set.

Results and discussion

CoMFA model

CoMFA analysis was performed to explore the structure–activity relationships of substituents on the phenyl ring and urea N–H group in 4-benzylpipridinealkylureas and amides as CCR3 antagonists. The structure and experimental values of activity, ranging from 0.005 μM to 1.6 μM, for the 41 molecules used in this study are shown in Table 1 [21]. The data set was divided into a training set of 32 molecules and a test set of 9 molecules according to structural diversity and activity range. During the rigorous cycle of model development and validation, we found two outlier molecules, **10** and **35**, that do not fit into the training or test set. Initially, CoMFA analysis was performed on a data set of 41 molecules with inclusion of molecules **10** and **35** in the training set. Many models were generated by taking various combinations of training and test set molecules. It was observed that inclusion of molecules **10** and **35** in the training set drastically decreases r^2_{cv} , which in turn decreases the robustness of the model. Therefore these molecules (**10** and **35**) were included in the test set to construct the CoMFA model. Their inclusion in the test set led to improvement in r^2_{cv}, but the model showed poor predictive power with high residual for molecules **10** (−1.01) and **35** (−0.90) (Table 1). The predictive power (r^2_{pred}) of the developed CoMFA model is low, having a value of 0.262. In addition, the developed model also has high value of PRESS (2.713), which signifies that the model was not significant. A possible explanation for such behaviour is that, in molecule **10**, inclusion of one sp^3 carbon (methylene group) between the urea NH group and the phenyl ring may change the orientation of the phenyl ring with respect to the rest of the molecules in the data set, whereas molecule **35** has a methyl group at a position *para* to the benzyl group in 4-benzylpiperidinealkylureas, which is different from the rest of the molecules in the data set, and is also a weak CCR3 antagonist.

To improve the prediction of the two outliers (**10** and **35**), a "systematic conformation approach" was performed by allowing a 10^o increment on all freely rotatable bonds of the substituted side chain, while keeping the conformation of the common scaffold fixed. This conformational search generates a satisfactory number of conformations on these molecules, and the conformation that showed good prediction with the least residual values of molecules **10** (0.56) and **35** (0.45) were selected. The selected conformation also showed good alignment with the template molecule **32**, and is presented in supplementary material Fig. S1a, b. This in turn significantly improved the PRESS (1.399) and predictivity r^2_{pred} (0.619) of the developed CoMFA model. The PLS analysis of the best CoMFA model is presented in Table 2. The constructed CoMFA model is robust with r^2_{cv} of 0.589 and conventional r^2 of 0.960, with five optimum NOC. The r^2_{cv} represents goodness of internal prediction, whereas r^2 represents the goodness of fit of a QSAR model. The standard error of estimate of the developed model is 0.155. The external predictive capability of a QSAR model is generally checked using test set molecules. The statistical

Table 2 Partial least squares (PLS) summary of CoMFA results. *S* Steric field, *E* electrostatic field, r^2_{cv} cross-validated correlation coefficient by PLS leave-one-out (LOO) method, *NOC* optimum number of components, *SEE* standard error of estimate, r^2 conventional correlation coefficient, r^2_{bs} correlation coefficient after 100 runs of bootstrapping, SD_{bs} standard deviation from 100 runs of bootstrapping, r^2_{pred} predictive correlation coefficient

Statistical parameter	CoMFA model
Number of molecules in training set	32
Number of molecules in test set	9
$r^2_{cv}(q^2)$	0.589
NOC	5
r^2	0.960
SEE	0.155
F-test	125.7
r^2_{bs}	0.986
SD_{bs}	0.007
r^2_{pred}	0.619
PRESS	1.399
Fraction of field contributions	
Steric	0.513
Electrostatic	0.487

validity and stability of the CoMFA model was assessed further by running bootstrap analysis for 100 runs. The higher r^2_{bs} value of 0.986 obtained after 100 runs of bootstrapping supports this analysis [25]. The scatter plots for actual versus predicted activities of training and test set molecules are shown in Fig. 3. Table 1 shows the structures and the corresponding IC_{50} (μM), actual and predicted pIC_{50} values of the molecules under study for CoMFA model development. All the aligned molecules are shown in Fig. 1.

Contour map analysis

CoMFA models are usually represented as 3D coefficient contour maps surrounding all lattice points where QSAR is found to deal strongly with changes in interaction energy or binding affinity with respect to structural changes. In other words, contour maps show how variation in steric or electrostatic properties of the structural features of molecules contained in the training set leads to an increase or decrease in activity. The polyhedra produced surround lattice points where the scalar products of the associated QSAR coefficient and the standard deviation of all values in the corresponding column of the data matrix are higher or lower than a user-specified value. SYBYL settings used different colours to represent electrostatic (blue and red) and steric (yellow and green) contours. In the case of the electrostatic contour map, a region where negative charge

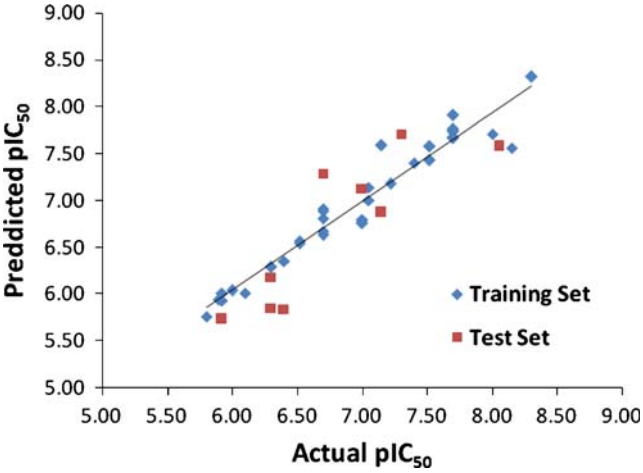

Fig. 3 Scatter plot of actual (experimental) activities versus comparative molecular field analysis (CoMFA) predicted activities of the training set (*blue points*) and test set (*magenta points*) molecules computed using CoMFA model

leads to increased activity is represented by red polyhedra, while a region with favourable positive charge is represented as a blue polyhedra. On the other hand, in the case of a steric map, yellow contours indicate regions that are sterically disfavoured, and addition of a bulky group at that point leads to a decrease in activity. While green contour regions represent sterically favoured points, bulky group substitution at these regions could lead to an increase in the activity of the molecule.

The total field contribution provided by the electrostatic field is 0.487, and by the steric field is 0.513, which implies

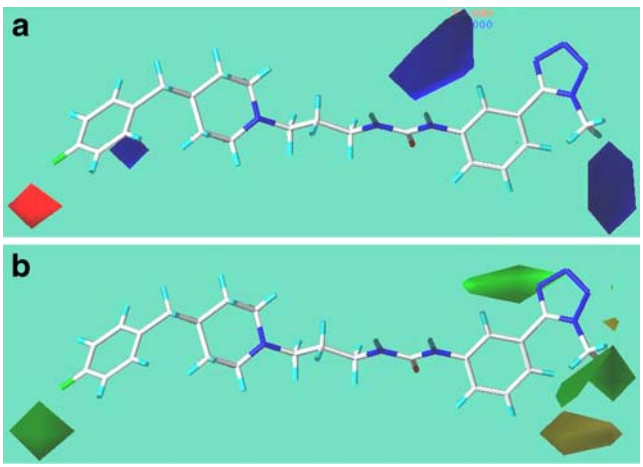

Fig. 4 CoMFA STDEV*COEFF electrostatic (**a**) and steric (**b**) contour maps of the most active molecule (**32**, shown in *capped stick* notation). **a** *Blue polyhedrons* Positive charge favoured areas (contribution level 80%), *red polyhedron* negative charge favoured areas (contribution level 20%). **b** *Green polyhedrons* Sterically favoured areas (contribution level 80%), *yellow polyhedrons* sterically disfavoured areas (contribution level 20%)

that the contribution of the steric part is predominant for interaction of these CCR3 antagonists. Contour map analysis was carried out by checking the orientation of the molecules in the contours, and observing the proximity of the relevant functionalities to those contours. From CoMFA contour analysis, it is obvious that the contours are distributed around substitutions at the 4th, 7th, 8th and 9th positions (Fig. 2) of the central core (4- benzylpiperidine alkylureas and amides).

The electrostatic and steric contours for the most active molecule (**32**) are displayed in Fig. 4a and b, respectively. The electrostatic contour map shown in Fig. 4a displays three blue polyhedra and one red polyhedron. The red contour near the 4th position of benzylpiperidine suggests that substitution of an electronegative group at this position leads to an increase in CCR3 antagonistic activity. This accounts for the greater activity of halogenated (**9**–**34**; **40**, **41**) to that of non-halogenated (**1**–**8**; **36**–**39**) benzylpiperidine molecules. The blue contour near the 8th position of the phenyl tetrazole ring shows that an electropositive group is required at this position for optimal activity. This explains the good activity of molecule **18**, which has a 4-nitro phenyl group at its R_2 position. The presence of a blue contour at the $–CH_3$ group of the 1-methyl tetrazole ring indicates that an electropositive group with optimal bulk is required to obtain more potent molecules.

CoMFA steric fields are predominant in these CCR3 antagonists (Table 2), hence the steric contour map will prove more useful to gain insight into the variation in biological activity with structural diversity. The steric contour plot presented in Fig. 4b shows a green contour surrounding the tetrazole group, indicating that bulky substituents at the 8th position of the phenyl tetrazole ring would be favourable. This accounts for the better activity of molecule **32** compared to that of the other molecules. The bulky group at the 8th position also increases the CCR3 antagonist activity of molecule **32** in comparison to other molecules, where there is a complete absence of this group. Contour map analysis near the region of the 9th position and the $–CH_3$ group of the 1-methyl tetrazole ring showed the presence of two medium sized green contours, indicating that substitution of a bulky group in this position may improve CCR3 antagonistic activity. This region also showed a yellow contour below it, which suggests that substitutions having optimal steric bulk or substitutions oriented away from the yellow contour are favoured. Therefore, the $–CH_3$ group can be substituted with $–C_2H_5$, $–CH(CH_3)_2$, etc. to obtain molecules with improved affinity and potency. Additionally, the medium-sized green polyhedron on the lower left side near the region at the 4th position suggests that this region would prefer bulky substituents such as Cl, CF_3, and CCl_3, and is presented in Fig. 4b.

Conclusions

3D-QSAR models for 41 4-benzylpiperidinealkylureas and amides of CCR3 antagonists were developed using the CoMFA technique. The best CoMFA model gave a cross-validated r^2_{cv} value of 0.589, a non cross-validated r^2 value of 0.960, and predicted r^2_{pred} value of 0.619 respectively. The model also showed good predictive power with low residuals for test set molecules. Thus, information gathered from the 3D-QSAR contribution maps shed some light on the effects of substitution patterns in relation to CCR3 antagonist activity.

Thus, the ligand-based 3D-QSAR model described herein will constitute a valuable tool for the rational design of novel, structurally related 4-benzylpiperidinealkylureas and amide antagonists, endowed with increased affinity towards CCR3.

Acknowledgements The authors are thankful to the Department of Pharmaceuticals, Govt. of India, for financial support. V.J. and A.P. gratefully acknowledge financial support received from the department in the form of a Junior Research Fellowship. S.G. is the recipient of a Senior Research Fellowship from the Council of Scientific and Industrial Research (New Delhi).

References

1. Gleich GJ, Adolphson CR (2000) The eosinophil and asthma. In: Busse WW, Holgate ST (eds) Asthma and rhinitis, 2nd edn. Blackwell, Oxford, pp 419–470
2. Gleich GJ (1990) The eosinophil and bronchial asthma: current understanding. J Allergy Clin Immunol 85:422–436
3. Griffiths-Johnson DA, Collins PD, Rossi AG, Jose PJ, Williams TJ (1993) The chemokine, eotaxin, activates guinea-pig eosinophils in vitro and causes their accumulation into the lung in vivo. Biochem Biophys Res Commun 197:1167–1172
4. Kampen GT, Stafford S, Adachi T, Jinquan T, Quan S, Grant JA, Skov PS, Poulsen LK, Alam R (2000) Eotaxin induces degranulation and chemotaxis of eosinophils through the activation of ERK2 and p38 mitogen-activated protein kinases. Blood 95:1911–1917
5. Murphy PM, Baggiolini M, Charo IF, Hebert CA, Horuk R, Matsushima K, Miller LH, Oppenheim JJ, Power CA (2000) International union of pharmacology. XXII nomenclature for chemokine receptors. Pharmacol Rev 52:145–176
6. Zlotnik A, Yoshie O (2000) Chemokines: a new classification system and their role in immunity. Immunity 12:121–127
7. Bertrand CP, Donath PD (2000) CCR3 blockade as a new therapy for asthma. Expert Opin Invest Drugs 9:43–52
8. Duchesnes CE, Murphy PM, Williams TJ, Pease JE (2006) Alanine scanning mutagenesis of the chemokine receptor CCR3 reveals distinct extracellular residues involved in recognition of the eotaxin family of chemokines. Mol Immunol 43:1221–1231
9. Wise EL, Duchesnes C, da Fonseca PCA, Allen RA, Williams TJ, Pease JE (2007) Small compound receptor agonists and antagonists of CCR3 provide insight into mechanisms of chemokine receptor activation. J Biol Chem 282:27935–27943
10. Berger EA, Murphy PM, Farber JM (1999) Chemokine receptors as HIV-1 coreceptors: roles in viral entry, tropism, and disease. Annu Rev Immunol 17:657–700

11. Alkhatib G, Berger EA, Murphy PM, Pease JE (1997) Determinants of HIV-1 coreceptor function on CC chemokine receptor 3, importance of both extracellular and transmembrane/cytoplasmic regions. J Biol Chem 272:20420–20426
12. Boehme SA, Sullivan SK, Crowe PD, Santos M, Conlon PJ, Sriramarao P, Bacon KB (1999) Activation of mitogen-activated protein kinase regulates eotaxin-induced eosinophil migration. J Immunol 163:1611–1618
13. El-Shazly A (2003) Basic concepts in eosinophil recruitment to sites of allergic inflammation: an in vitro model of the pathophysiology of late response in allergic rhinitis. Int Congr Ser 1240:1081–1086
14. Pease JE, Wang J, Ponath PD, Murphy PM (1998) The N-terminal extracellular segments of the chemokine receptors CCR1 and CCR3 are determinants for MIP-1alpha and eotaxin binding, respectively, but a second domain is essential for efficient receptor activation. J Biol Chem 273:19972–19976
15. Vedani A, Dobler M, Dollinger H, Hasselbach KM, Birke F, Lill MA (2005) Novel ligands for the chemokinereceptor-3 (CCR3):a receptor-modeling study based on 5D-QSAR. J Med Chem 48:1515–1527
16. Kubinyi H (2006) Special Publication. Royal Society of Chemistry 304:219–240
17. Awale M, Mohan CG (2008) Molecular docking guided 3D-QSAR CoMFA analysis of N-4-pyrimidinyl-1H-indazol-4-amine inhibitors of leukocyte-specific protein tyrosine kinase. J Mol Model 14:937–947
18. Awale M, Mohan CG (2008) 3D QSAR CoMFA analysis of C5 substituted pyrrolotriazines as HER2 (ErbB2) inhibitors. J Mol Graph Model 26:1169–1178
19. Garg D, Gandhi T, Mohan CG (2008) Exploring QSTR and toxicophore of hERG K+ channel blockers using GFA and HypoGen techniques. J Mol Graph Model 26:966–976
20. Wold S, Johansson A, Cochi M (1993) In: Kubinyi H (ed) 3D QSAR in drug design: theory, methods and applications. ESCOM, Lieden, pp 523–550
21. Wacker DA, Santella IJ, Gardner DS, Varnes JG, Estrella M, DeLucca GV, Ko SS, Tanabe K, Watson PS, Welch PK (2002) CCR3 antagonists: a potential new therapy for the treatment of asthma. Discovery and structure-activity relationships. Bioorg Med Chem Lett 12:1785–1789
22. Cramer RD III, Patterson DE, Bunce JD (1988) Effect of shape on binding of steroids to carrier proteins. J Am Chem Soc 110:5959–5967
23. SYBYL7.1, Tripos Inc, St Louis, MO
24. Clark M, Cramer RD, Van Opdenbosch N (1989) Validation of the general purpose tripos 5.2 force field. J Comput Chem 10:982–1012
25. Cramer RD, Bunce JD, Patterson DE, Frank IE (1988) Cross validation, bootstrapping and partial least squares compared with multiple regression in conventional QSAR studies. Quant Struct Act Relat 7:18–25